Article

A Novel Strategy for Automatic Mode Pairing on the Model Updating of Railway Systems with Nonproportional Damping

Diogo Ribeiro [1,*], Cássio Bragança [2], Maik Brehm [3], Volkmar Zabel [4] and Rui Calçada [5]

1   CONSTRUCT-LESE, School of Engineering, Polytechnic of Porto, 4249-015 Porto, Portugal
2   Department of Structural Engineering, Federal University of Minas Gerais, Belo Horizonte 31270-901, Brazil
3   Merkle CAE Solutions GmbH, 89518 Heidenheim, Germany
4   Institute of Structural Mechanics, Bauhaus-University Weimar, 99423 Weimar, Germany
5   CONSTRUCT-LESE, Faculty of Engineering, University of Porto, 4200-465 Porto, Portugal
*   Correspondence: drr@isep.ipp.pt

Abstract: Mode pairing is a crucial step for the stability of any model-updating strategy based on experimental modal parameters. Automatically establishing a stable and assertive correspondence between numerical and experimental modes, in many cases, proves to be a very challenging task, especially in situations where complex mode shapes are present. This article presents a novel formulation for the automatic mode pairing between experimental and numerical complex modes based on an Energy-based Modal Assurance Criterion (EMAC). The efficiency of the proposed criterion was demonstrated on the basis of a case study involving the pairing between numerical and experimental modes of a passenger railway vehicle. A highly complex detailed FE numerical model of the vehicle was developed involving the modeling of the carbody, bogies and axles. A numerical damped modal analysis allowed obtaining the main global rigid-body and flexural modes of the vehicle's carbody, as well as several local modes associated to the vibration of specific components of the carbody. Due to the localized damping provided by the suspensions, these modes presented complex modal ordinates, especially for the rigid-body modes. The comparison between the results obtained from the application of the EMAC and the classical MAC criteria, on the pairing of five global mode shapes, proved that the EMAC criterion is much more assertive, avoiding mismatches between the experimental global modes and some of the local numerical modes with similar configurations, and, consequently, establishing the correct correspondences between experimental and numerical modes.

Keywords: model updating; automatic mode pairing; complex modal parameters; energy-based MAC

1. Introduction

The overall use of numerical modeling techniques based on the finite element (FE) method, as well as experimental techniques for operational modal analysis (OMA), made the updating of numerical models based on modal parameters quite widespread [1]. These model-updating methodologies are widely used for: (i) developing highly accurate numerical models [2–6]; (ii) modeling structures under operational conditions with unknown levels of degradation and/or geometrical/mechanical parameters with very high levels of uncertainty [7,8]; (iii) monitoring the evolution of the structural behavior during retrofit operations [9]; and (iv) identifying structural damage [10,11], among others.

In most situations, these methodologies are based on the minimization of an objective function, composed by the residuals between numerical and experimental modal parameters, through the iterative variation of sensitive parameters of the numerical model [4]. During the optimization process, particularly due to variations on the numerical parameters' values, several changes in the order of the numerical mode shapes are frequently registered. To guarantee that these modifications do not affect the search for the optimal solution, it must be ensured that, in all iterations throughout the optimization process, the residuals of the objective function are calculated between an experimental mode and its

correspondent numerical counterpart. Thus, the convergence of the optimization problem fundamentally depends on an efficient, automatic and stable mode-pairing technique to perform the correct assignment between numerical and experimental modes [12].

Most of the mode-pairing techniques are based on metrics for evaluating the correlation between two vectors (in this case, modal ordinate vectors), or between Frequency Response Functions (FRFs) [13,14]. Such metrics, applied to experimental and numerical results, allow to quantify the degree of correlation between the modes, and, consequently, to assign each experimental mode to its numerical counterpart [12]. The metrics based on FRFs are less widespread in the field of mode pairing compared to those based on modal ordinate vectors, mainly due to the difficulties associated with the estimation of the experimental FRFs in large-scale structures. Nevertheless, the Frequency Domain Assurance Criterion (FDAC), proposed by [15], can be used for mode pairing with FRFs. The FDAC computes the correlation between two FRFs for different frequency shifts, and provides, for each frequency, a scalar between 0 and 1, with 0 meaning no correspondence and 1 meaning full correspondence.

Among the modal-ordinate-vector-based criteria, one of the first to be applied is known as the Modal Scale Factor (MSF), proposed by [16]. The MSF is defined as the inner product of the two modal ordinate vectors to be compared, scaled by the inner product of either one of these vectors, making it significantly dependent on the normalization of the modes [17]. This dependence on the normalization factor sometimes causes a problem in practical applications, since it is often not possible to apply the same normalization to experimental and numerical modes, especially when using OMA techniques to gather experimental data. A very widespread criterion that is independent from normalization is the Modal Assurance Criterion (MAC), proposed by [16]. The MAC is defined as the square of the inner product of the two vectors, scaled by the product of the two inner products of the two vectors by themselves, resulting in a real scalar between 0 and 1 [18].

Based on the MAC, several other criteria for the correlation between modal ordinate vectors were proposed: the Partial MAC (PMAC) [19], in which only part of the modal ordinate vector is used in the calculations, focusing the analysis in a particular component or direction; the Extended MAC (MACX) [20], with an expanded assertiveness for complex modes, and its enhanced version (MACXP) [20], which, by a weighting with the poles of the corresponding mode shapes, improves the performance of the criterion under reduced spatial resolution; and the Weighted MAC (WMAC), also known as Normalized Cross Orthogonality (NCO), which incorporates the mass or stiffness matrices as a weighting matrix for the calculation of the MAC, remedying the shortcoming of the MAC not being a true orthogonality check [13]. However, due to the fact that usually not all degrees of freedom are instrumented, the application of the WMAC requires condensing the mass or stiffness matrices through model-reduction techniques [13,17]. Another issue regarding the WMAC is that, for complex mode shapes, a different formulation based on the state formulation of the orthogonality condition is required. This is due to the orthogonality conditions with respect to mass and stiffness matrices not being met for complex modes [21].

The mathematical formulation of some of these criteria will be briefly presented in Section 2 of the manuscript. A more detailed description of these and other criteria can be consulted, for example, in the References section [17,19,21,22].

A common issue associated with the application of these classic mode-pairing criteria arises when dealing with structures where local modes are associated to a particular structural component, as well as a set of components or parts of the structure that do not constitute the object of interest but also have global components, even if very small, with a shape similar to the true global modes. These modes, especially when they have close natural frequencies, can easily generate errors in the matching process and compromise the stability of the model-optimization algorithm [12,23].

Seeking to solve this issue, Brehm et al. [12] proposed an innovative criterion, the EMAC, which is based on the weighting of the MAC by the relative modal strain energy associated with different parts of the structure denominated as clusters. The authors

demonstrated that, through the appropriate choice of clusters, it is possible to isolate modes from different parts of the structure quite efficiently. Applications of the EMAC for mode pairing can be consulted in the works of [3,5,23,24], in which its use proved to be essential in applications involving the model updating of FE models of railway bridges including the track.

Since it relies on the orthogonality conditions between the vibration modes and the stiffness matrix to calculate the modal strain energy, the EMAC, according to its original formulation, cannot be applied to problems involving complex modes. In many cases, especially in civil engineering structures where the modes are real or almost real, this does not represent a problem, and often, the pairing and model updating are performed considering the undamped modal problem. However, in the case of vehicles and structures with localized dampers, modes with a significant degree of complexity are present. In these situations, the EMAC ends up being at a disadvantage compared to criteria such as the FDAC, the MSF and the MAC, which can be applied to complex modes, and even more in relation to the MACX, which was specifically developed for these applications.

In this framework, the present work intends to share innovative contributions that, according to the authors' knowledge, are not sufficiently detailed in the existing literature, namely:

- The development of a mode-pairing formulation dedicated to complex modes based on an energy-based criterion and relying on a state-space formulation. The existing criteria for complex mode shapes reveal weaknesses and tend to fail in several situations;
- The evaluation of the performance of the developed mode-pairing criterion based on a case study involving a highly complex FE model of a railway vehicle and experimental modal parameters. In the existing mode pairing criteria, the validation is usually performed based on simple numerical or analytical examples. Additionally, the experimental restrictions associated with the positioning and number of sensors, noise and environmental interference create more challenging conditions to evaluate the performance of the pairing criteria.

This article presents the main existing mode-pairing criteria for complex modes, with a special emphasis on the criteria relying on the Energy-based Modal Assurance Criteria (EMAC). Regarding the EMAC, an innovative mathematical formulation based on a state-space model is detailed. Then, this criterion was applied to a case study involving the automatic mode pairing between the experimental and numerical modes of a passenger railway vehicle. In railway vehicles, the localized damping introduced by the suspension systems is responsible for the existence of complex mode shapes. In addition, the numerical model considers the flexibility of the carbody's elements, and consequently, the local modes of the panels that form the floor, walls and roof are present. These two aspects make the application of a criterion such as the EMAC particularly relevant to obtain a stable and robust automatic mode pairing.

2. Review of Existing Mode-Pairing Criteria

In this section, some of the most used criteria for mode pairing, which can be applied for systems with complex modes, are briefly presented. In addition to their mathematical formulation, the advantages and disadvantages of using each of these criteria are also presented.

2.1. Modal Assurance Criterion (MAC)

The Modal Assurance Criterion (MAC) is the most used criterion for pairing numerical and experimental modes of vibration [17,21,25]. It is defined as:

$$\mathrm{MAC}_{ij} = \frac{\left|\mathbf{\Phi}_i^H \mathbf{\Phi}_j\right|^2}{\mathbf{\Phi}_i^H \mathbf{\Phi}_i \mathbf{\Phi}_j^H \mathbf{\Phi}_j} \tag{1}$$

in which $\boldsymbol{\Phi}_i$ and $\boldsymbol{\Phi}_j$ are the vectors containing the modal ordinates of modes i and j, respectively, and ^{H} is the Hermitian transpose (conjugate transpose) operator.

According to [12], the main advantages of applying the MAC parameter are: (i) simple implementation; (ii) experimental information is not required on all degrees of freedom of the structure; and (iii) it does not depend on the normalization of the modal vectors. However, according to [21], the value of the MAC parameter strongly depends on the dimension of the modal vectors and is also particularly sensitive to the change in the higher amplitude ordinates. Due to these issues, pairing by the MAC value may be not sufficient in cases of complex structures, as well as in continuous structures or structures with partial continuity, such as bridges with several spans, as demonstrated by [23]. Examples of the application of the MAC criterion in mode pairing can be found in references [1,2,26,27].

2.2. Extended Modal Assurance Criterion (MACX)

As stated by Sternharz et al. [22], the MAC criteria might lead to inconclusive results in the case of modes with a significant level of complexity, especially in the presence of close or repeated modes. According to Vacher et al. [20], these inconclusive results are due to the fact that the MAC provides different results depending on the combinations made with the pairs of complex and complex-conjugate of the two mode shapes being compared. In order to address those issues, Vacher et al. [20] proposed the Extended Modal Assurance Criterion (MACX), defined as:

$$\text{MACX}_{ij} = \frac{\left(\left| \boldsymbol{\Phi}_i^H \boldsymbol{\Phi}_j \right| + \left| \boldsymbol{\Phi}_i^T \boldsymbol{\Phi}_j \right| \right)^2}{\left(\boldsymbol{\Phi}_i^H \boldsymbol{\Phi}_i + \left| \boldsymbol{\Phi}_i^T \boldsymbol{\Phi}_i \right| \right) \left(\boldsymbol{\Phi}_j^H \boldsymbol{\Phi}_j + \left| \boldsymbol{\Phi}_j^T \boldsymbol{\Phi}_j \right| \right)} \tag{2}$$

in which ^{T} is the transpose operator.

Compared to the MAC, the use of the MACX provides more consistent results in the case of complex mode shapes, but it is also influenced by the dimension of the modal ordinate vector and more sensible to variations in components of greater amplitude. Examples of its application can be found in references [28,29].

Aiming to improve the MACX performance in situations where the modal ordinate vectors contain information from only a few points, Vacher et al. [20] proposed an enhancement of the criterion called Pole-Weighted MACX (MACXP). This criterion incorporates information regarding the natural frequencies and damping ratios of the structure by weighting the MACX with the poles of the dynamic system.

The MACXP is defined as:

$$\text{MACXP}_{ij} = \frac{\left(\frac{\left| \boldsymbol{\Phi}_i^H \boldsymbol{\Phi}_j \right|}{\left| \lambda_i^* + \lambda_j \right|} + \frac{\left| \boldsymbol{\Phi}_i^T \boldsymbol{\Phi}_j \right|}{\left| \lambda_i + \lambda_j \right|} \right)^2}{\left(\frac{\boldsymbol{\Phi}_i^H \boldsymbol{\Phi}_i}{2 \left| \text{Re}(\lambda_i) \right|} + \frac{\left| \boldsymbol{\Phi}_i^T \boldsymbol{\Phi}_i \right|}{2 \left| \lambda_i \right|} \right) \left(\frac{\boldsymbol{\Phi}_j^H \boldsymbol{\Phi}_j}{2 \left| \text{Re}(\lambda_j) \right|} + \frac{\left| \boldsymbol{\Phi}_j^T \boldsymbol{\Phi}_j \right|}{2 \left| \lambda_j \right|} \right)} \tag{3}$$

in which λ_i and λ_j are the poles associated with modes i and j, and * is the complex-conjugate operator. It was demonstrated by Vacher et al. [20] that this weighting by the poles is capable of significantly improving the accuracy of the criterion in situations where there are few sample points. Examples of the application of this criterion can be consulted in [22].

2.3. Frequency Domain Assurance Criterion (FDAC)

The Frequency Domain Assurance Criterion (FDAC), proposed by Pascual et al. [15], is analogous to the MAC criteria, but it is calculated with the Frequency Response Functions (FRFs) with distinct frequency shifts. It is defined as:

$$\text{FDAC}\left(\omega_f, \omega_g\right) = \frac{\left|\sum_{p=1}^{N}\sum_{q=1}^{N} h_{pq}^{(x)}\left(\omega_f\right) h_{pq}^{*(a)}\left(\omega_g\right)\right|^2}{\left(\sum_{p=1}^{N}\sum_{q=1}^{N} h_{pq}^{(x)}\left(\omega_f\right) h_{pq}^{*(x)}\left(\omega_f\right)\right)\left(\sum_{p=1}^{N}\sum_{q=1}^{N} h_{pq}^{(a)}\left(\omega_g\right) h_{pq}^{*(a)}\left(\omega_g\right)\right)} \tag{4}$$

in which $h_{pq}^{(x)}\left(\omega_f\right)$ and $h_{pq}^{(a)}\left(\omega_g\right)$ are the values of the FRFs corresponding to an excitation at the Degree Of Freedom (DOF) p, measured at DOF q and at frequencies ω_f and ω_g, respectively [30]. The FDAC parameter allows for the analysis of the correspondence between two FRFs for all frequencies within a selected range. Such an operation results in something similar to a MAC matrix, although it is much denser given the large number of frequency values which can be used compared to the restricted number of modes used to compute the MAC matrix [13].

Several variants of this criterion are also found in the literature, such as the Response Vector Assurance Criterion (RVAC) [31], in which only one column of the FRF matrix is used to compute the FDAC; the improved FDAC [15], which takes into account the lags between the FRFs and prevents the pairing of FRFs with a lag of 180°; and the complex FDAC [30], which is calculated without the modulus and conjugated operator in the numerator to account for the real and imaginary parts of the criterion.

The major drawbacks associated with the application of this mode-pairing criteria are related to the necessity of estimating experimental FRFs, which are not obtained when applying OMA techniques. Furthermore, the FDAC calculation implies a higher computational cost compared to the correlation criteria between modal order vectors, especially when there is a wide range and high resolution of frequencies. Examples of application of the FDAC criteria and its variants are found in references [32–34].

3. Mode Pairing Using the Energy-Based Modal Assurance Criterion (EMAC)

An efficient and robust mode-pairing criterion is a key aspect to assure the stability of any model-updating methodology based on experimental modal data. Undoubtedly, the MAC is the most used criterion for this task. However, due to its drawbacks (presented in Section 2), it might be unsuitable in some situations. Some of these issues may be solved by a proper weighting of the MAC values. The criterion based on strain energy gathers the information from the mathematical correlation between the modal vectors with the physical information of the degrees of freedom observed in the dynamic test and related to the stiffness or mass distribution.

In this criterion, the correspondence of the numerical modes with the experimental ones is carried out through the EMAC parameter (Energy-based Modal Assurance Criterion) which is given by:

$$\text{EMAC}_{ijk} = \prod{}_{jk}\text{MAC}_{ij} \tag{5}$$

This parameter results from the weighting of the MAC parameter by the relative modal strain energy ($\prod_{jk}$) of one or several groups of degrees of freedom of the numerical model, called clusters. Each experimental mode is paired with the numerical mode corresponding to the highest value of the EMAC parameter.

The success of the criterion based on the EMAC parameter largely depends on the selection of the degrees of freedom of the numerical model that form the various clusters. Clusters must allow for the separation of measured degrees of freedom from unmeasured degrees of freedom in the test. In complex structures, the clusters must also consider the different substructures constituted by groups of elements with a dynamic behavior different from the global structure.

This criterion was developed and successfully applied by Brehm et al. [12] for the case of real vibration modes. Its application to complex vibration modes based on a state-space formulation is innovative and is not reported in the bibliography in detail.

In this section, the mathematical formulation of the EMAC criterion is presented. First, the formulation proposed by Brehm et al. [12] for real modes is briefly presented, as it represents the basis for the understanding of the formulation for complex modes. Then, the mathematical formulation of the newly innovative approach to dealing with complex modes is presented.

3.1. Real Modes

In the case of real vibration modes, the relative modal strain energy uses the physical information of the stiffness matrix. Its calculation involves rearranging the modal vectors and dividing the stiffness matrix into submatrices that relate the different clusters [12].

Assuming that the modal matrix ($\boldsymbol{\Phi}$) is normalized in relation to the mass matrix, the modal stiffness matrix, which constitutes the orthogonality condition in relation to the stiffness matrix, is as follows:

$$\boldsymbol{\Phi}^T \mathbf{K} \boldsymbol{\Phi} = \begin{bmatrix} \ddots & & \\ & \omega_j^2 & \\ & & \ddots \end{bmatrix} \tag{6}$$

in which ω_j corresponds to the angular natural frequency of mode j. The total strain energy (Modal Strain Energy) associated with each vibration mode j (MSE$_j$) is equal to $1/2 \times \omega_j^2$.

The vector that contains the modal information of the numerical mode j can be rearranged by separating the degrees of freedom of the numerical model into n clusters:

$$\boldsymbol{\Phi}_j^T = \left[\boldsymbol{\Phi}_{j1}^T \boldsymbol{\Phi}_{j2}^T \cdots \boldsymbol{\Phi}_{jn}^T \right]^T \tag{7}$$

In turn, the stiffness matrix is also divided into submatrices ($\mathbf{K}_{kl}$) that relate the degrees of freedom of clusters k and l, that is:

$$\mathbf{K} = \begin{bmatrix} \mathbf{K}_{11} & \mathbf{K}_{12} & \cdots & \mathbf{K}_{1n} \\ \mathbf{K}_{21} & \mathbf{K}_{22} & \cdots & \mathbf{K}_{2n} \\ \vdots & \vdots & \ddots & \vdots \\ \mathbf{K}_{n1} & \mathbf{K}_{n2} & \cdots & \mathbf{K}_{nn} \end{bmatrix} \tag{8}$$

where k and l take values equal to 1, 2, ..., n, and n is the total number of clusters.

The modal strain energy of vibration mode j with respect to cluster k (MSE$_{jk}$) is calculated based on the following expression:

$$\mathrm{MSE}_{jk} = \frac{1}{2} \sum_{l=1}^{n} \boldsymbol{\Phi}_{jk}^T \mathbf{K}_{kl} \boldsymbol{\Phi}_{jl} \tag{9}$$

where $\boldsymbol{\Phi}_{jk}$ is the matrix that contains the modal information of the numerical mode j, corresponding to the degrees of freedom of cluster k; $\mathbf{K}_{kl}$ is the stiffness submatrix that relates the degrees of freedom of clusters k and l; and $\boldsymbol{\Phi}_{jl}$ is the matrix that contains the modal information of numerical mode j, corresponding to the degrees of freedom of cluster l.

The total strain energy of vibration mode j is given by:

$$\mathrm{MSE}_j = \frac{1}{2} \sum_{k=1}^{n} \sum_{l=1}^{n} \boldsymbol{\Phi}_{jk}^T \mathbf{K}_{kl} \boldsymbol{\Phi}_{jl} = \frac{1}{2} \boldsymbol{\Phi}_j^T \mathbf{K} \boldsymbol{\Phi}_j = \frac{1}{2} \omega_j^2 \tag{10}$$

The relative strain energy ($\prod_{jk}$) represents the portion of the total energy mobilized by the vibration mode j considering only the degrees of freedom of cluster k. It can be calculated based on Equations (9) and (10), that is:

$$\prod_{jk} = \frac{\text{MSE}_{jk}}{\text{MSE}_j} = \frac{\sum_{l=1}^{n} \mathbf{\Phi}_{jk}^T \mathbf{K}_{kl} \mathbf{\Phi}_{jl}}{\mathbf{\Phi}_j^T \mathbf{K} \mathbf{\Phi}_j} \tag{11}$$

with $\text{MSE}_j \neq 0$. This parameter is a scalar that takes values in the range between 0 and 1. Finally, the EMAC_{ijk} is calculated through Equation (5).

3.2. Complex Modes

In cases where the damping matrix is not proportional to the mass and stiffness matrices, the so-called complex modes of vibration are present. These are characterized by complex numbers, i.e., they encompass both magnitude and phase information. In a complex vibration mode, the movements of the points occur with a time delay proportional to the phase difference, situated between $0°$ and $180°$. The representation of the deformed structure is usually performed with animations that present the values of the amplitudes of the various components of the modes at different instants of time [17].

In the case of complex vibration modes, the previously presented formulation cannot be directly applied since the orthogonality conditions with respect to the stiffness matrix (Equation (6)) are not met. Therefore, to obtain an expression for the modal strain energy it is necessary to resort to a formulation based on state-space equations.

In a state-space formulation, the system of second-order differential equilibrium equations, with dimension z, is transformed into a system of $2z$ first-order differential equations. To this end, the state vector $\mathbf{x}(t)$ is defined with z lines, which are constituted by the displacements and velocities of the z degrees of freedom of the structure:

$$\mathbf{x}(t) = \begin{bmatrix} \mathbf{q}(t) \\ \dot{\mathbf{q}}(t) \end{bmatrix} \tag{12}$$

Based on the state-space formulation, the equation of motion ($\mathbf{M}\ddot{\mathbf{q}} + \mathbf{C}\dot{\mathbf{q}} + \mathbf{K}\mathbf{q} = \mathbf{p}(t)$) can be rewritten as:

$$\mathbf{P}\dot{\mathbf{x}}(t) + \mathbf{Q}\mathbf{x}(t) = \begin{Bmatrix} \mathbf{p}(t) \\ 0 \end{Bmatrix} \tag{13}$$

$\mathbf{P}$ and $\mathbf{Q}$ are defined in Equations (14) and (15), respectively, in terms of the stiffness, damping and mass matrices [35,36]:

$$\mathbf{P} = \begin{bmatrix} \mathbf{C} & \mathbf{M} \\ \mathbf{M} & 0 \end{bmatrix} \tag{14}$$

$$\mathbf{Q} = \begin{bmatrix} \mathbf{K} & 0 \\ 0 & -\mathbf{M} \end{bmatrix} \tag{15}$$

Assuming $q(t) = \varphi_j e^{\lambda_j t}$ as a solution for homogeneous differential equations results in the following eigenvalue problem:

$$\mathbf{Q} \cdot \mathbf{\Psi} = -\mathbf{P} \cdot \mathbf{\Psi} \cdot \mathbf{\Lambda_C} \tag{16}$$

The eigenvalues ($\mathbf{\Lambda}$) and the eigenvectors ($\mathbf{\Psi}$) can be related to matrices that contain the vibration modes ($\mathbf{\Theta}$) and λ_j, which characterize the dynamic behavior of the structure through the following expressions:

$$\mathbf{\Lambda_C} = \begin{bmatrix} \mathbf{\Lambda} & 0 \\ 0 & \mathbf{\Lambda}^* \end{bmatrix} \tag{17}$$

$$\mathbf{\Psi} = \begin{bmatrix} \mathbf{\Theta} & \mathbf{\Theta}^* \\ \mathbf{\Theta\Lambda} & \mathbf{\Theta}^*\mathbf{\Lambda}^* \end{bmatrix} \tag{18}$$

where

$$\mathbf{\Lambda} = \begin{bmatrix} \ddots & & \\ & \lambda_j & \\ & & \ddots \end{bmatrix} \qquad j = 1, \ldots, n \tag{19}$$

$$\mathbf{\Theta} = \begin{bmatrix} \ldots & \mathbf{\Phi}_j & \ldots \end{bmatrix} \qquad j = 1, \ldots, n \tag{20}$$

in which $\mathbf{\Phi}_j$ is a vector containing the modal ordinates of mode i, and λ_i is the associated eigenvalue [35,36].

Based on the previously presented formulation, the following orthogonality conditions can be derived:

$$\mathbf{\Psi}^{\mathrm{T}}\mathbf{P}\mathbf{\Psi} = \begin{bmatrix} \ddots & & \\ & a_j & \\ & & \ddots \end{bmatrix} \tag{21}$$

$$\mathbf{\Psi}^{\mathrm{T}}\mathbf{Q}\mathbf{\Psi} = \begin{bmatrix} \ddots & & \\ & b_j & \\ & & \ddots \end{bmatrix} \tag{22}$$

in which a_j and b_j play a role similar to the modal mass and modal stiffness for undamped vibration systems but are usually complex numbers [36]. Therefore, in the case of complex modes, the modal strain energy can be calculated based on the second orthogonality condition, and the total strain energy associated with mode j (MSE_j) is equal to $1/2 \times b_j$.

The matrix $\mathbf{\Psi}$ has a dimension of $2z \times 2n'$, where z is the number of degrees of freedom of the numerical model and n' is the total number of vibration modes. This matrix can be rearranged by separating the degrees of freedom of the numerical model into n clusters, resulting in:

$$\mathbf{\Psi} = \begin{bmatrix} \mathbf{\Phi}_{11} & \mathbf{\Phi}_{12} & \cdots & \mathbf{\Phi}_{1n'} & \mathbf{\Phi}_{11}^* & \mathbf{\Phi}_{12}^* & \cdots & \mathbf{\Phi}_{1n'}^* \\ \mathbf{\Phi}_{21} & \mathbf{\Phi}_{22} & \cdots & \mathbf{\Phi}_{2n'} & \mathbf{\Phi}_{21}^* & \mathbf{\Phi}_{22}^* & \cdots & \mathbf{\Phi}_{2n'}^* \\ \vdots & \vdots & \ddots & \vdots & \vdots & \vdots & \ddots & \vdots \\ \mathbf{\Phi}_{n1} & \mathbf{\Phi}_{n2} & \cdots & \mathbf{\Phi}_{nn'} & \mathbf{\Phi}_{n1}^* & \mathbf{\Phi}_{n2}^* & \cdots & \mathbf{\Phi}_{nn'}^* \\ \mathbf{\Phi}_{11}\lambda_1 & \mathbf{\Phi}_{12}\lambda_2 & \cdots & \mathbf{\Phi}_{1n'}\lambda_{n'} & \mathbf{\Phi}_{11}^*\lambda_1^* & \mathbf{\Phi}_{12}^*\lambda_2^* & \cdots & \mathbf{\Phi}_{1n'}^*\lambda_{n'}^* \\ \mathbf{\Phi}_{21}\lambda_1 & \mathbf{\Phi}_{22}\lambda_2 & \cdots & \mathbf{\Phi}_{2n'}\lambda_{n'} & \mathbf{\Phi}_{21}^*\lambda_1^* & \mathbf{\Phi}_{22}^*\lambda_2^* & \cdots & \mathbf{\Phi}_{2n'}^*\lambda_{n'}^* \\ \vdots & \vdots & \ddots & \vdots & \vdots & \vdots & \ddots & \vdots \\ \mathbf{\Phi}_{n1}\lambda_1 & \mathbf{\Phi}_{n2}\lambda_2 & \cdots & \mathbf{\Phi}_{nn'}\lambda_{n'} & \mathbf{\Phi}_{n1}^*\lambda_1^* & \mathbf{\Phi}_{n2}^*\lambda_2^* & \cdots & \mathbf{\Phi}_{nn'}^*\lambda_{n'}^* \end{bmatrix} \tag{23}$$

The vector that contains the modal information of the numerical mode j can be rearranged by separating the degrees of freedom of the n clusters. It has the following format:

$$\mathbf{\Psi}_j^T = \begin{bmatrix} \mathbf{\Phi}_{1j}^T \mathbf{\Phi}_{2j}^T \cdots \mathbf{\Phi}_{nj}^T (\mathbf{\Phi}_{1j}\lambda_j)^T (\mathbf{\Phi}_{2j}\lambda_j)^T \cdots (\mathbf{\Phi}_{nj}\lambda_j)^T \end{bmatrix}^T \tag{24}$$

In turn, the matrix $\mathbf{Q}$, with a dimension of $2z \times 2z$, is also divided into submatrices ($\mathbf{K}_{kl}$ and $\mathbf{M}_{kl}$) that relate the degrees of freedom of clusters k and l, that is:

$$\mathbf{Q} = \begin{bmatrix} \mathbf{K}_{11} & \mathbf{K}_{12} & \cdots & \mathbf{K}_{1n} & 0 & 0 & \cdots & 0 \\ \mathbf{K}_{21} & \mathbf{K}_{22} & \cdots & \mathbf{K}_{2n} & 0 & 0 & \cdots & 0 \\ \vdots & \vdots & \ddots & \vdots & \vdots & \vdots & \ddots & \vdots \\ \mathbf{K}_{n1} & \mathbf{K}_{n2} & \cdots & \mathbf{K}_{nn} & 0 & 0 & \cdots & 0 \\ 0 & 0 & \cdots & 0 & -\mathbf{M}_{11} & -\mathbf{M}_{12} & \cdots & -\mathbf{M}_{1n} \\ 0 & 0 & \cdots & 0 & -\mathbf{M}_{21} & -\mathbf{M}_{12} & \cdots & -\mathbf{M}_{2n} \\ \vdots & \vdots & \ddots & \vdots & \vdots & \vdots & \ddots & \vdots \\ 0 & 0 & \cdots & 0 & -\mathbf{M}_{n1} & -\mathbf{M}_{n2} & \cdots & -\mathbf{M}_{nn} \end{bmatrix} \tag{25}$$

in which k and l can assume values equal to 1, 2, ..., n, where n is the total number of clusters.

Based on this submatrix division of $\mathbf{Q}$, it is possible to form the matrices $\mathbf{Q}_{kl}$, which relate the degrees of freedom from clusters k and l, that is:

$$\mathbf{Q}_{kl} = \begin{bmatrix} \mathbf{K}_{kl} & 0 \\ 0 & -\mathbf{M}_{kl} \end{bmatrix} \tag{26}$$

Therefore, the modal strain energy from mode j with respect to cluster k (MSE_{jk}) can be calculated by:

$$\mathrm{MSE}_{jk} = \frac{1}{2} \sum_{l=1}^{n} \mathbf{\Psi}_{jk}^{T} \mathbf{Q}_{kl} \mathbf{\Psi}_{jl} \tag{27}$$

where $\mathbf{\Psi}_{jk}$ is the matrix that contains the information of numerical mode j, corresponding to the degrees of freedom of cluster k; $\mathbf{Q}_{kl}$ is the submatrix from $\mathbf{Q}$ relating the degrees of freedom from clusters k and l; and $\mathbf{\Psi}_{jl}$ is the matrix containing the modal information of numerical mode j, corresponding to the degrees of freedom from cluster l.

The total modal strain energy of mode j is given by:

$$\mathrm{MSE}_{j} = \frac{1}{2} \sum_{k=1}^{n} \sum_{l=1}^{n} \mathbf{\Psi}_{jk}^{T} \mathbf{Q}_{kl} \mathbf{\Psi}_{jl} = \frac{1}{2} \mathbf{\Psi}_{j}^{T} \mathbf{Q} \mathbf{\Psi}_{j} = \frac{1}{2} b_{j} \tag{28}$$

Therefore, the relative strain energy ($\prod_{jk}$) represents the portion of the total energy mobilized by vibration mode j considering only the degrees of freedom of cluster k. It is given by:

$$\prod_{jk} = \frac{\left| \mathrm{MSE}_{jk} \right|}{\left| \mathrm{MSE}_{j} \right|} = \frac{\left| \sum_{l=1}^{n} \mathbf{\Psi}_{jk}^{T} \mathbf{Q}_{kl} \mathbf{\Psi}_{jl} \right|}{\left| \mathbf{\Psi}_{j}^{T} \mathbf{Q} \mathbf{\Psi}_{j} \right|} \tag{29}$$

with $\mathrm{MSE}_{j} \neq 0$. Similarly to the case involving real modes, the relative strain energy ($\prod_{jk}$) varies from 0 to 1.

4. Case Study

In this section, the presented EMAC formulation for complex modes is applied to a case study involving the mode pairing between numerical and experimental modes of a BBN tourist-class passenger railway vehicle. The BBN vehicle (Figure 1) is a 25.9 m and 55-ton car with two motor bogies and capacity for 62 passengers. This vehicle is part of the CPA 4000 series ("Alfa Pendular") train which operates in the line connecting the cities of Porto and Lisbon in Portugal.
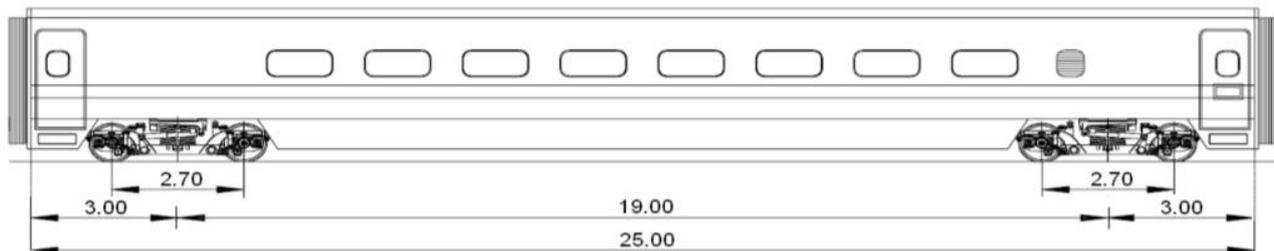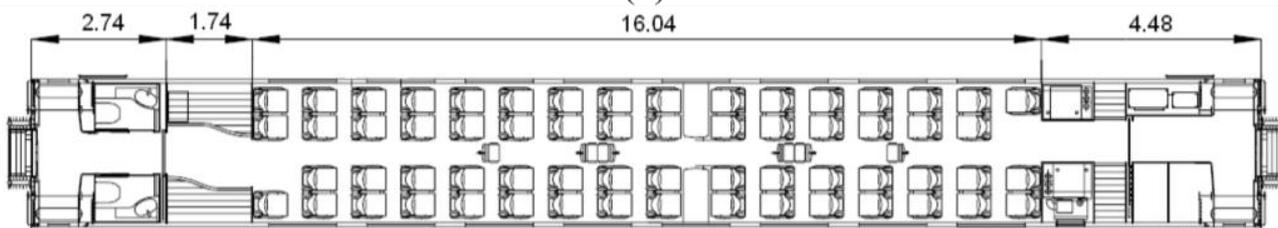
Figure 1. BBN vehicle: (**a**) perspective; (**b**) elevation; (**c**) floor plan.

4.1. Numerical Model

The numerical model of the vehicle (Figure 2) was developed based on shell, beam and spring-dashpot assemblies. Particularly, the beam elements were used for modeling the bogies, and the spring-dashpot assemblies were used to simulate the suspensions, the connecting rods and the tilting system. The shell elements were used to model the floor, the roof and the wall panels. The thickness of the shell elements was considered to match the cross-sectional area with one of the real panels. The real panels, however, are formed by an upper and lower plate connected by diagonal plates, thus presenting an orthotropic behavior to bending. To adequately represent this behavior, the inertia of the shell elements was corrected by the RMI (Ratio of the Bending Moment of Inertia) [37] parameter given by the ratio between the real inertia of the panel and that given by the shell element.
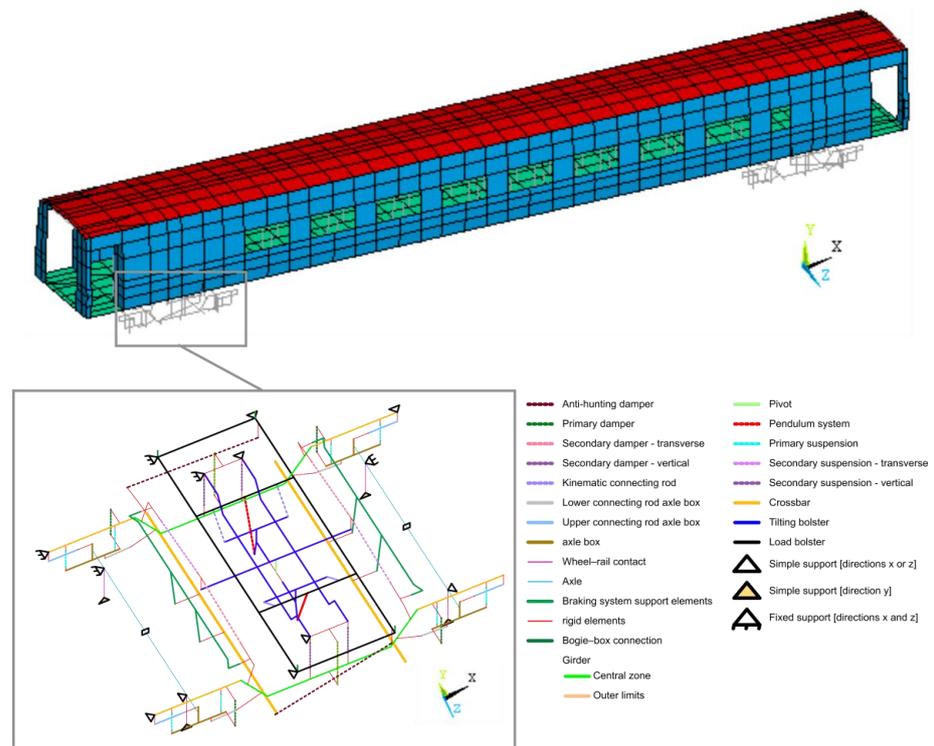
Figure 2. Overview of the BBN vehicle's numerical model.

The main parameters of the numerical model are depicted in Table 1, according to the information provided by the manufacturer of the BBN vehicle.

Table 1. Main parameters of the BBN vehicle's numerical model.

Parameter	Designation		Adopted Value	Unit
	Carbody			
K_{S1}	Vertical secondary suspension stiffness	Front bogie	256.4	kN/m
K_{S2}		Rear bogie		
c_S	Vertical secondary suspension damping		35	kNm/s
K_{ST}	Transverse secondary suspension stiffness		2500	kN/m
c_{ST}	Transverse secondary suspension damping		17.5	kNm/s
K_{Pend}	Rigidity of the pendulum system		0 (at rest)	kN/m
c_{AL}	Anti-hunting suspension damping		400	kNm/s
K_b	Stiffness of the tilting bolster–load bolster connection rod		20,000	kN/m
Δ_{alum}	Aluminum density		2700	kg/m^3
E_{alum}	Aluminum deformability module	Dir x	70	GPa
		Dir z	54.2	GPa
RMI_b	Corrective factor of the moment of inertia	Floor	90	-
RMI_p		Walls	114	-
RMI_c		Roof	386	-
ΔM_b	Additional mass	Floor	70	%
ΔM_p		Walls	20	%
ΔM_c		Roof	10	%

Table 1. *Cont.*

Parameter	Designation		Adopted Value	Unit
e_{bas}	Equivalent thickness	Floor	10.2	mm
e_{par}		Walls	10.3	mm
e_{cob}		Roof	8.8	mm
Bogies				
K_P	Primary suspension stiffness		564	kN/m
c_P	Primary suspension damping		18	kNm/s
K_{bls}	Axle-box connecting rod stiffness	Top	6.5	MN/m
K_{bli}		Bottom	25	MN/m
K_{rc}	Stiffness of the wheel–rail contact		1.5674×10^9	N/m
ΔM_{lc}	Additional mass	Girder (central zone)	42	kg/m
ΔM_{le}		Girder (extremities)	38	kg/m
ΔM_t		Crossmember	92	kg/m
ΔM_e		Axles	271	kg/m

Additionally, concentrated mass elements were used to incorporate the mass of some non-structural components and equipment at the wagon's floor and at specific locations distributed along the bogies. The adequate positioning of these elements is essential for accurately representing the vehicle's modal behavior. The positioning and corresponding values of these masses are depicted in Figure 3.


- Air-conditioning system: 2 units of 360 kg
- Transmission: 2 units of 90 kg
- Active suspension controller: 2 units of 67 kg
- Traction engine and radiator: 2 units of 985 kg
- Tilting system controller: 1 unit of 380 kg
- Braking system controller: 1 unit of 447 kg
- Reservoirs (full): 2 units of 375 kg
- Braking indicator: 2 units of 20 kg
- Traction converter: 2350 kg
- Traction converter radiator: 880 kg

(a)

- Support system for the anti-hunting damper and support crossmember for the brake discs: 6 units of 50 kg
- Lower steering rod support system of the axle box: 4 units of 10 kg
- Upper steering rod support system of the axle box: 4 units of 10 kg
- Side-stop support system: 2 units of 10 kg
- Brake discs: 5 units of 100 kg
- Gearbox: 1 unit of 346 kg
- Wheelset: 4 units of 263 kg

(b)

Figure 3. Mass elements in the finite element model: (**a**) carbody; (**b**) bogie.

Figure 4 depicts the modal configurations and natural frequencies of the vehicle's carbody. Among the rigid-body modes, 1C is a rotation about the *x* axis, 2C is a translation along the *y* axis, and 3C is a rotation about the *z* axis. Due to the relevant contribution of the localized damping provided by the suspension elements, these rigid-body modes presented a high degree of complexity. Among the deformation modes, 4C and 6C are, respectively, the first and second torsional modes, and 5C is the first bending mode.

Mode 1C
f = 0.86 Hz

Mode 2C
f = 1.04 Hz

Mode 3C
f = 1.42 Hz

Mode 4C
f = 10.21 Hz

Mode 5C
f = 16.20 Hz

Mode 6C
f = 15.05 Hz
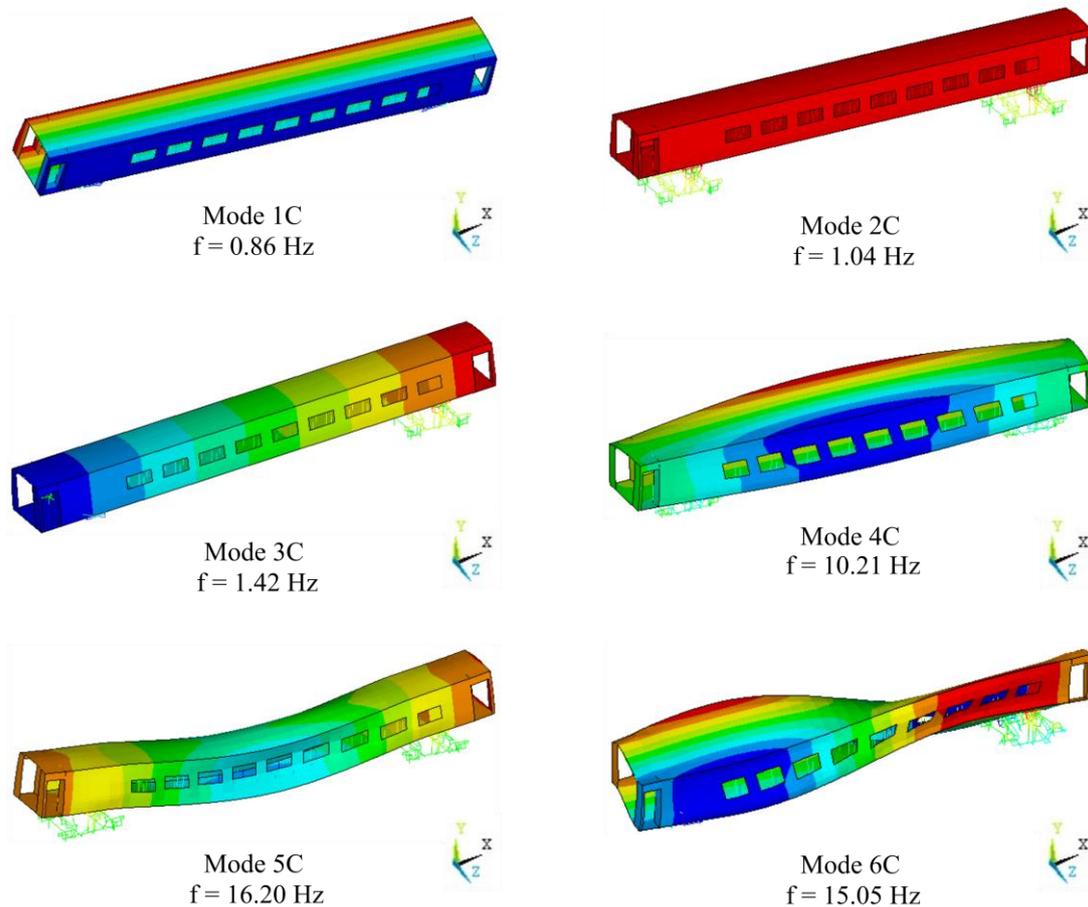
Figure 4. Numerical modes of the BBN vehicle's carbody.

Several local modes involving the bending of elements of the box, in particular the base, walls and roof, were also identified. As an example, Figure 5 illustrates the first two local modes (1L and 2L) that involve bending movements of the base of the carbody, with natural frequencies of the damped system equal to 8.85 Hz and 9.63 Hz, respectively.

Mode 1L
f = 8.85 Hz

Mode 2L
f = 9.63 Hz
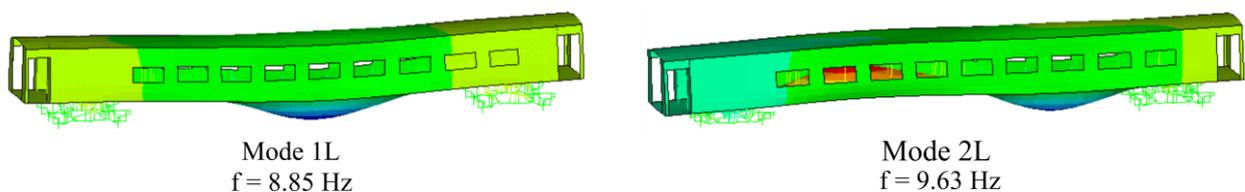
Figure 5. Numerically obtained local vibration modes of the housing.

As can be seen in Figure 5, despite being clearly local, modes 1L and 2L contain global displacement components, which might be confused with global modes and create extra difficulties for an automatic mode-pairing algorithm. Particularly, in Mode 1L, these global movements are very similar, in a smaller scale, to the first global bending mode (5C).

The vehicle damping matrix was constructed as the sum of a Rayleigh damping matrix and the matrix resulting from the scattering of the matrices of the elements with localized damping, particularly the primary, secondary and anti-hunting dampers. The addition of the matrices from the localized dampers to the Rayleigh damping matrix makes it nonproportional to the stiffness and mass matrices, which results in complex modes.

The Rayleigh constants were calculated setting damping coefficients equal to 2% for the 4C and 6C vibration modes. The evolution of the damping coefficient as a function of frequency for the Rayleigh damping portion is graphically represented in Figure 6.
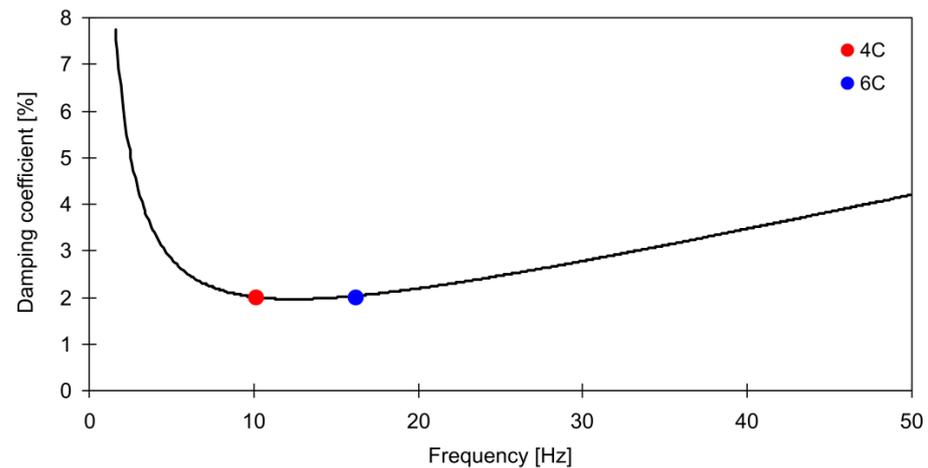
Figure 6. Rayleigh damping curve.

4.2. Mode Pairing

A dynamic test, described in detail in [4], was performed based on a set of 14 accelerometers distributed along the floor of the carbody. The tests allowed for the identification of 5 experimental vibration modes, depicted in Figure 7, which clearly correspond to the numerical modes 1C to 5C previously presented in Figure 4. In Figure 7, for each vibration mode, the respective natural frequency and Mode Complexity Factor (MCF) [38] are also indicated.

Mode 1C
f = 1.01 Hz | MCF = 14.60 %

Mode 2C
f = 1.33 Hz | MCF = 7.05 %

Mode 3C
f = 1.59 Hz | MCF = 16.92 %

Mode 4C
f = 8.38 Hz | MCF = 68.80 %

Mode 5C
f = 12.26 Hz | MCF = 17.80 %
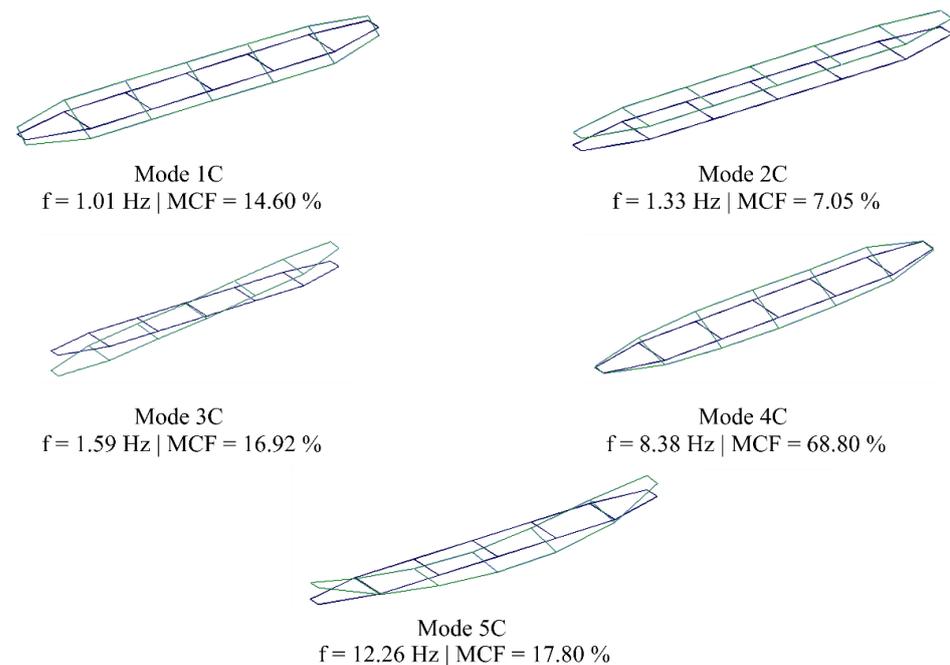
Figure 7. Experimental carbody modes.

To demonstrate the performance of the EMAC in automatically pairing these experimental modes to their numerical correspondents, the vehicle's FE model was divided into the four clusters presented in Figure 8. The carbody clusters, namely the floor, walls and roof, where each split into sub-clusters containing only the degrees of freedom associated with the vertical (*y*) and transverse (*z*) directions, respectively. Accordingly, seven separate clusters were obtained in total. In the "other elements" cluster, the remaining degrees of freedom of translation and rotation of the numerical model were included, encompassing, among others, the bogies and the seats.
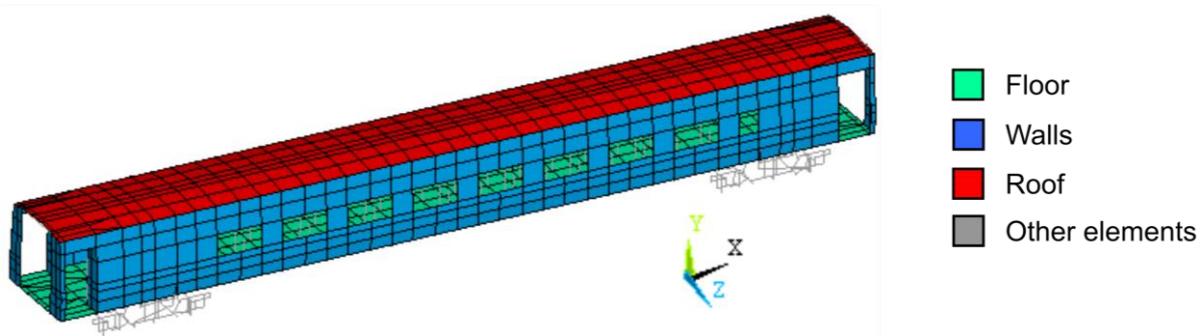
Figure 8. Identification of the clusters used in the numerical model of the BBN vehicle.

For each of these clusters, the relative modal strain energy (see Figure 9) was calculated through Equation (29) considering 80 vibration modes, obtained through a numerical modal analysis taking the damping into account.
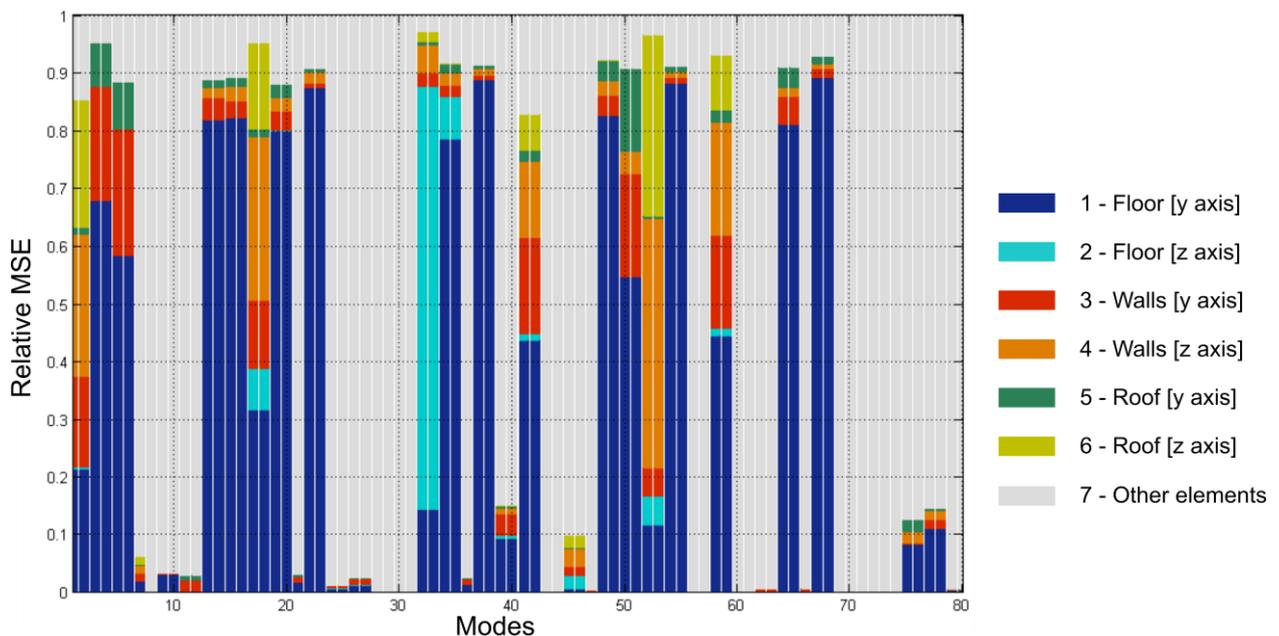
Figure 9. Relative MSE values for the different clusters and vibration modes, obtained based on the numerical model of the BBN vehicle.

Figure 10 presents the MAC and EMAC correlation matrices between the 80 numerical modes and the 5 experimentally identified modes (see Figure 7). In this Figure, the 80 numerical modes correspond to 40 complex-conjugate pairs. The EMAC values for the 2C, 3C and 5C modes were obtained by weighting the MAC by the modal strain energy of the clusters 1, 3 and 5 (see Figures 8 and 9). The EMAC values for the 1C and 4C modes resulted of the weighting of the MAC values by the modal strain energy of the clusters 1, 4 and 6 (see Figures 8 and 9). Cluster 1 is representative of the positioning of the sensors

and the measurement direction used in the dynamic test of the carbody, since the sensors were installed on the vehicle's floor. The use of other clusters in the weighting of the MAC values, particularly in the rigid-body modes, allowed to highlight the interrelationship between the degrees of freedom of the base, walls and roof in the *y* and *z* directions.


(a)

(b)
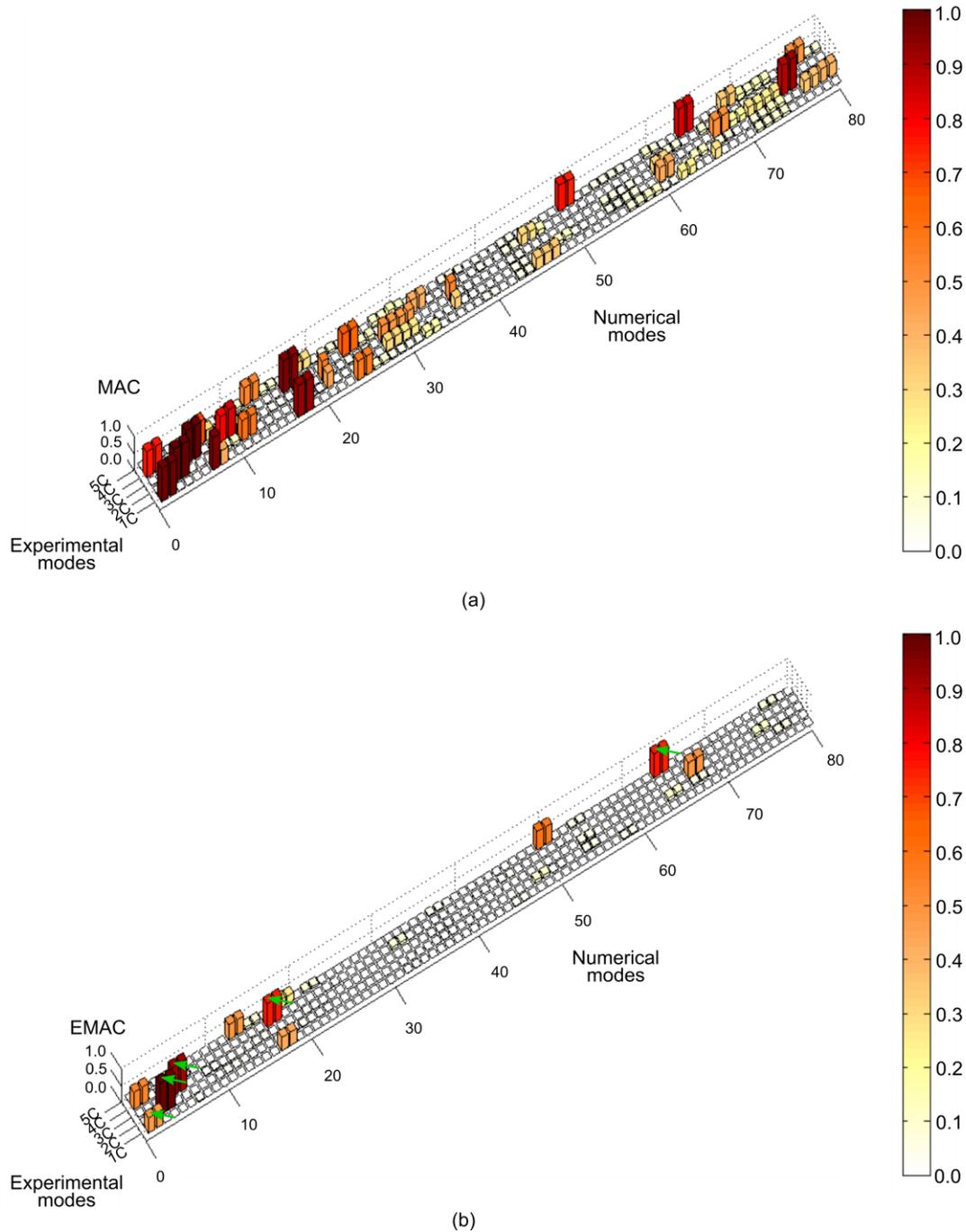
Figure 10. Pairing of experimental and numerical modes of the BBN vehicle based on the (**a**) MAC and (**b**) EMAC parameters.

As can be clearly seen, the EMAC matrix is significantly cleaner compared to the MAC matrix. The application of the EMAC allowed for the proper pairing the between experimental and numerical modes, as indicated by the little green arrows in Figure 10b. On the other hand, the use of the MAC parameter resulted in a high level of correlation

between the experimental modes and several numerical modes, which made it impossible to establish a proper pairing between experimental and numerical modes.

The EMAC parameter facilitated the pairing of the 1C and 5C experimental modes, especially. Figure 11 shows two numerical vibration modes, modes 7 and 50, which can be paired with experimental modes 1C and 5C, respectively, and which the use of the EMAC parameter allowed to exclude. Mode 7 is a transverse rotation mode of both bogies. It causes small-amplitude transverse-rotation movements of the box. Mode 50 is a global bending mode with local-box base movements.

Numerical mode 7
(f = 4.89 Hz; MAC = 0.948)

(a)

Numerical mode 50
(f = 14.20 Hz; MAC = 0.766)

(b)
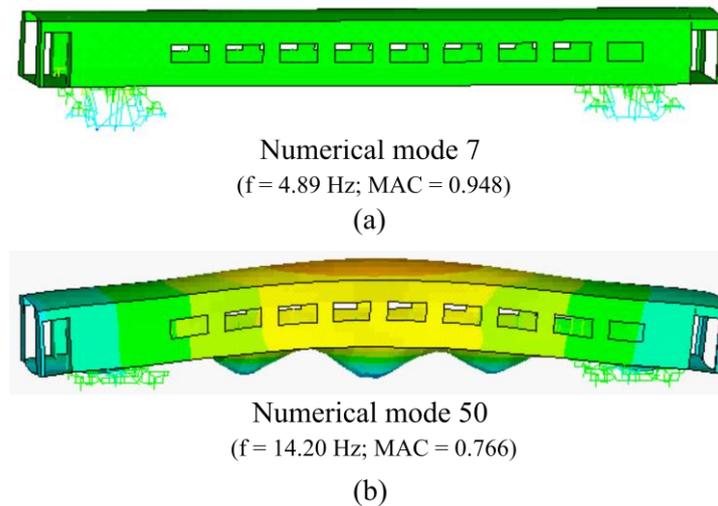
Figure 11. Numerical vibration modes likely to pair with (**a**) experimental mode 1C, and (**b**) experimental mode 5C.

It is also important to highlight the significant correlation between vibration modes 1C and 4C. As can be seen from Figure 7, due to the limited number of points where the experimental information was available, the deformed modal configurations of these two modes, from the perspective of the instrumented points, are very similar. The distinction between these two modes became more evident using the EMAC parameter.

5. Conclusions

This paper presents a novel approach to the problem of automatic pairing complex vibration modes through the expansion of the MAC criterion weighted by the modal strain energy (EMAC), for its application in problems involving complex mode shapes.

To enable the application of the EMAC to problems with complex modes, an expression for the modal strain energy was derived on the basis of the orthogonality conditions of a state-space formulation. The derived formulation allows to quantify the relative modal strain energy, used for the weighting of the MAC, in cases where the orthogonality condition between the modes and the stiffness matrix is not satisfied. Consequently, this made it possible to expand the criterion to more general applications.

Subsequently, the effectiveness of the proposed criterion was demonstrated through a case study involving the pairing of modes of a BBN-type passenger vehicle. A detailed numerical model of the vehicle was developed in ANSYS® based on shell, beam, spring-dashpot assemblies and concentrated mass elements. Particularly, the shell elements were used to represent the panels of the carbody, the beam elements were used to model the bogies, the spring-dashpot assemblies were used to model the suspension components, and the mass elements were used to represent the non-structural equipment and components of the vehicle. The localized damping effect introduced by the dampers led to a non-proportional damping matrix and, consequently, to complex modes.

A numerical modal analysis was performed, in which it was possible to identify the main rigid-body modes of the carbody in addition to the first structural modes associated

with the bending and torsional movements of the carbody. In addition to these global modes, it was possible to identify several local modes, mainly for bending the carbody panels. These modes presented global components of small amplitude with a format very similar to some of the global modes, which imposes extra difficulties in the pairing process.

The numerical modes were paired with five experimental modes, from which information was available on the modal ordinate amplitudes of the 14 points that were instrumented on the vehicle floor. To demonstrate the efficiency of the proposed criterion, the pairing process was performed by the MAC and EMAC, with the aim of comparing the results obtained. After applying both criteria, the EMAC proved to be much more assertive in establishing the correct correspondences between numerical and experimental modes, even in challenging situations, due to the reduced number and positioning constraints of the sensors and the complexity of the numerical model. The weighting by the modal deformation energy, used in the EMAC, was able to significantly reduce the erroneous correspondences between the experimental global modes and the purely local modes verified when applying the MAC. In addition, even more assertive results are expected in situations with a higher number of sensors and larger spatial distribution.

In conclusion, the new formulation proposed for the application of the EMAC criterion to complex modes has proved to be very promising and represents an advance for future applications involving the updating of numerical models in the presence of non-proportional damping conditions.

Institutional Review Board Statement: Not applicable.

Informed Consent Statement: Not applicable.

Data Availability Statement: Data is unavailable due to privacy restrictions.

Conflicts of Interest: The authors declare no conflict of interest.

References

1. Bragança, C.; Neto, J.; Pinto, N.; Montenegro, P.A.; Ribeiro, D.; Carvalho, H.; Calçada, R. Calibration and Validation of a Freight Wagon Dynamic Model in Operating Conditions Based on Limited Experimental Data. *Veh. Syst. Dyn.* **2022**, *60*, 3024–3050. [CrossRef]
2. Silva, R.; Ribeiro, D.; Bragança, C.; Costa, C.; Arêde, A.; Calçada, R. Model Updating of a Freight Wagon Based on Dynamic Tests under Different Loading Scenarios. *Appl. Sci.* **2021**, *11*, 10691. [CrossRef]
3. Ribeiro, D.; Calçada, R.; Delgado, R.; Brehm, M.; Zabel, V. Finite Element Model Updating of a Bowstring-Arch Railway Bridge Based on Experimental Modal Parameters. *Eng. Struct.* **2012**, *40*, 413–435. [CrossRef]
4. Ribeiro, D.; Calçada, R.; Delgado, R.; Brehm, M.; Zabel, V. Finite-Element Model Calibration of a Railway Vehicle Based on Experimental Modal Parameters. *Veh. Syst. Dyn.* **2013**, *51*, 821–856. [CrossRef]
5. Meixedo, A.; Ribeiro, D.; Calçada, R.; Delgado, R. Global and Local Dynamic Effects on a Railway Viaduct with Precast Deck. In Proceedings of the 2nd International Conference on Railway Technology: Research, Development and Maintenance, Ajaccio, France, 8–11 April 2014. [CrossRef]
6. Ribeiro, D.; Bragança, C.; Costa, C.; Jorge, P.; Silva, R.; Arêde, A.; Calçada, R. Calibration of the Numerical Model of a Freight Railway Vehicle Based on Experimental Modal Parameters. *Structures* **2022**, *38*, 108–122. [CrossRef]
7. Clementi, F.; Pierdicca, A.; Formisano, A.; Catinari, F.; Lenci, S. Numerical Model Upgrading of a Historical Masonry Building Damaged during the 2016 Italian Earthquakes: The Case Study of the Podestà Palace in Montelupone (Italy). *J. Civ. Struct. Health Monit.* **2017**, *7*, 703–717. [CrossRef]

8. Costa, C.; Ribeiro, D.; Jorge, P.; Silva, R.; Arêde, A.; Calçada, R. Calibration of the Numerical Model of a Stone Masonry Railway Bridge Based on Experimentally Identified Modal Parameters. *Eng. Struct.* **2016**, *123*, 354–371. [CrossRef]

9. Pierdicca, A.; Clementi, F.; Fortunati, A.; Lenci, S. Tracking Modal Parameters Evolution of a School Building during Retrofitting Works. *Bull. Earthq. Eng.* **2019**, *17*, 1029–1052. [CrossRef]

10. Alves, V.N.; de Oliveira, M.M.; Ribeiro, D.; Calçada, R.; Cury, A. Model-Based Damage Identification of Railway Bridges Using Genetic Algorithms. *Eng. Fail. Anal.* **2020**, *118*, 104845. [CrossRef]

11. Huang, M.-S.; Gül, M.; Zhu, H.-P. Vibration-Based Structural Damage Identification under Varying Temperature Effects. *J. Aerosp. Eng.* **2018**, *31*, 04018014. [CrossRef]

12. Brehm, M.; Zabel, V.; Bucher, C. An Automatic Mode Pairing Strategy Using an Enhanced Modal Assurance Criterion Based on Modal Strain Energies. *J. Sound Vib.* **2010**, *329*, 5375–5392. [CrossRef]

13. Ewins, D.J. Model Validation: Correlation for Updating. *Sadhana Acad. Proc. Eng. Sci.* **2000**, *25*, 221–234. [CrossRef]

14. Lein, C.; Beitelschmidt, M. Comparative Study of Model Correlation Methods with Application to Model Order Reduction. In Proceedings of the ISMA 2014—International Conference on Noise and Vibration Engineering and USD 2014–International Conference on Uncertainty in Structural Dynamics, Leuven, Belgium, 15–17 September 2014; pp. 2683–2700.

15. Pascual, R.; Golinval, J.C.; Razeto, M. A Frequency Domain Correlation Techinique for Model Correlation and Updating. In Proceedings of the 15th International Modal Analysis Conference (IMAC XV), Orlando, FL, USA, 3–7 February 1997.

16. Allemang, R.J.; Brown, D.L. Correlation Coefficient for Modal Vector Analysis. In Proceedings of the International Modal Analysis Conference & Exhibit, Orlando, FL, USA, 6–9 February 1982; pp. 110–116.

17. Ewins, D.J. *Modal Testing: Theory, Practice and Application*, 2nd ed.; Wiley: Baldock, UK, 2009; ISBN 978-0863802188.

18. Pastor, M.; Binda, M.; Harčarik, T. Modal Assurance Criterion. *Procedia Eng.* **2012**, *48*, 543–548. [CrossRef]

19. Heylen, W.; Janter, T. Extensions of the Modal Assurance Criterion. *J. Vib. Acoust. Trans. ASME* **1990**, *112*, 468–472. [CrossRef]

20. Vacher, P.; Jacquier, B.; Bucharles, A. Extensions of the MAC Criterion to Complex Modes. In Proceedings of the ISMA 2010–International Conference on Noise and Vibration Engineering, including USD 2010, Leuven, Belgium, 20–22 September 2010; pp. 2713–2725.

21. Allemang, R.J. The Modal Assurance Criterion–Twenty Years of Use and Abuse. *Sound Vib.* **2003**, *37*, 14–21.

22. Sternharz, G.; Kalganova, T.; Mares, C.; Meyeringh, M. Comparative Performance Assessment of Methods for Operational Modal Analysis during Transient Order Excitation. *Mech. Syst. Signal Process.* **2022**, *169*, 108719. [CrossRef]

23. Ticona Melo, L.R.; Ribeiro, D.; Calçada, R.; Bittencourt, T.N. Validation of a Vertical Train–Track–Bridge Dynamic Interaction Model Based on Limited Experimental Data. *Struct. Infrastruct. Eng.* **2020**, *16*, 181–201. [CrossRef]

24. Ribeiro, D.; Calçada, R.; Brehm, M.; Zabel, V. Calibration of the Numerical Model of a Track Section over a Railway Bridge Based on Dynamic Tests. *Structures* **2021**, *34*, 4124–4141. [CrossRef]

25. Brehm, M. *Vibration-Based Model Updating: Reduction and Quantification of Uncertainties*; Bauhaus Universitat Weimar: Weimar, Germany, 2011.

26. Jaishi, B.; Ren, W.-X. Structural Finite Element Model Updating Using Ambient Vibration Test Results. *J. Struct. Eng.* **2005**, *131*, 617–628. [CrossRef]

27. Akiyama, Y.; Tomioka, T.; Takigami, T.; Aida, K.; Kamada, T. A Three-Dimensional Analytical Model and Parameter Determination Method of the Elastic Vibration of a Railway Vehicle Carbody. *Veh. Syst. Dyn.* **2020**, *58*, 545–568. [CrossRef]

28. Pereira, S.; Magalhães, F.; Gomes, J.P.; Cunha, Á. Modal Tracking under Large Environmental Influence. *J. Civ. Struct. Health Monit.* **2022**, *12*, 179–190. [CrossRef]

29. Bonisoli, E.; Lisitano, D.; Vigliani, A. Damping Identification and Localisation via Layer Method: Experimental Application to a Vehicle Chassis Focused on Shock Absorbers Effects. *Mech. Syst. Signal Process.* **2019**, *116*, 194–216. [CrossRef]

30. Pérez, M.A.; Serra-López, R. A Frequency Domain-Based Correlation Approach for Structural Assessment and Damage Identification. *Mech. Syst. Signal Process.* **2019**, *119*, 432–456. [CrossRef]

31. Van Der Auweraer, H.; Iadevaia, M.; Emborg, U.; Gustavsson, M.; Tengzelius, U.; Horlin, N. Linking Test and Analysis Results in the Medium Frequency Range Using Principal Field Shapes. In Proceedings of the the 23rd International Conference on Noise and Vibration Engineering, ISMA, Leuven, Belgium, 16–18 September 1998; pp. 129–136.

32. Cuadrado, M.; Pernas-Sánchez, J.; Artero-Guerrero, J.A.; Varas, D. Detection of Barely Visible Multi-Impact Damage on Carbon/Epoxy Composite Plates Using Frequency Response Function Correlation Analysis. *Measurement* **2022**, *196*, 111194. [CrossRef]

33. Pérez, M.A.; Manjón, A.; Ray, J.; Serra-López, R. Experimental Assessment of the Effect of an Eventual Non-Invasive Intervention on a Torres Guitar through Vibration Testing. *J. Cult. Herit.* **2017**, *27*, S103–S111. [CrossRef]

34. Pascual, R.; Razeto, M.; Golinval, J.C.; Schalchli, R. A Robust FRF-Based Technique for Model Updating. In Proceedings of the International Conference on Noise and Vibration Engineering ISMA, Leuven, Belgium, 16–18 September 2002; pp. 1037–1045.

35. Magalhães, F.M.R.L. *de Identificação Modal Estocástica Para Validação Experimental de Modelos Numéricos*; Universidade do Porto: Porto, Portugal, 2004.

36. Craig, R.R., Jr.; Kurdila, A.J. *Fundamentals of Structural Dynamics*, 2nd ed.; John Wiley & Sons: Hoboken, NJ, USA, 2006; ISBN 0471430447.

37. ANSYS Inc. *ANSYS®Theory Reference Manual*; ANSYS Inc: Canonsburg, PA, USA, 2007.
38. ARTeMIS. *ARTeMIS Extractor Pro–Academic License, User's Manual*; SVS: Aalborg, Denmark, 2009.